Outline

Show full outline

Figures (10)

1.

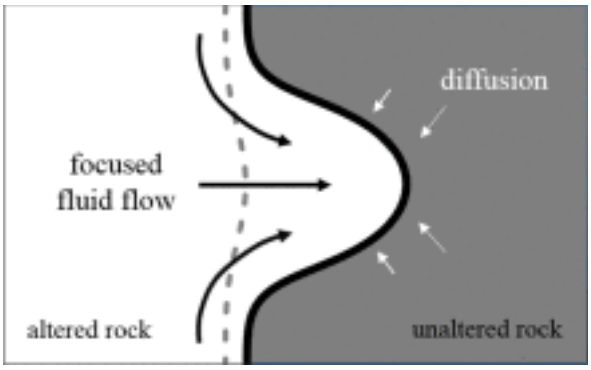

2.

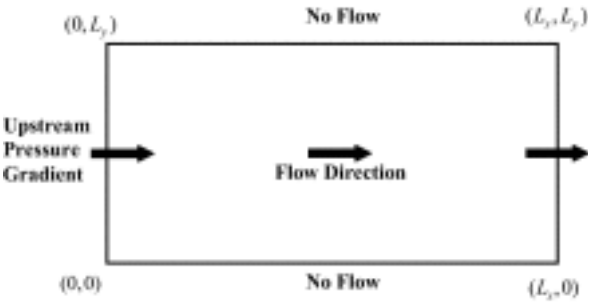

3.

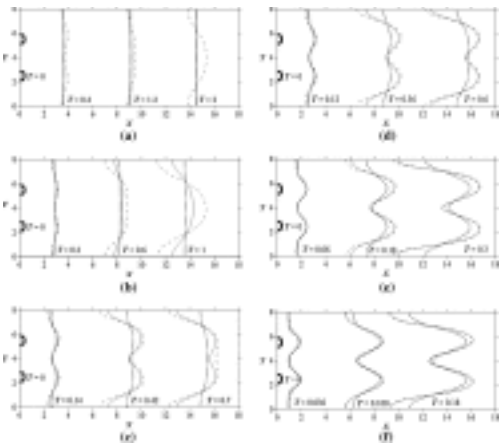

4.

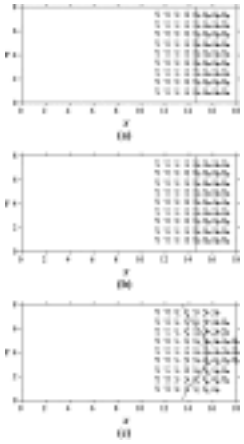

5.

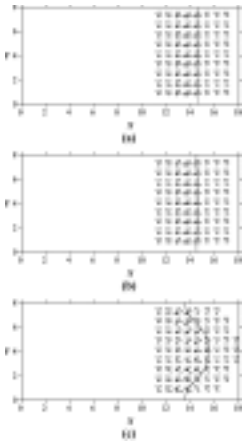

6.

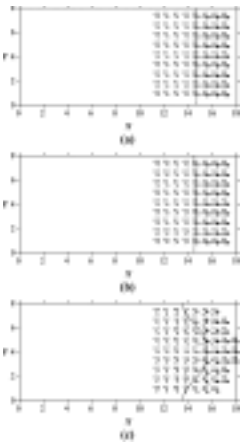

Show all figures

Journal of Hydrology
Volume 533, February 2016, Pages 224-233

Effect of medium permeability anisotropy on the morphological evolution of two non-uniformities in a geochemical dissolution system

Author links open overlay panelKeng-HsinLai[a]Jui-ShengChen[a]Chen-WuingLiu[b]Shao-YiuHsu[c]CarlSteefel[d]
Show more

https://doi.org/10.1016/j.jhydrol.2015.11.039Get rights and content

Highlights

- Effects of permeability anisotropy on chemical dissolution fronts.
- Permeability anisotropy modified flow-focusing effect.
- Permeability anisotropy influences morphologies of dissolution fronts.
- Effects of permeability anisotropy decrease when upstream pressure gradient increases.

Summary

The morphological evolutions of chemical dissolution fronts have attracted increasing interest in the field of the geological sciences and in industrial applications. Extensive research based on numerical simulations has been conducted to understand how various mechanisms and processes influence the morphological evolution of chemical dissolution fronts within geological media. Most researchers in previous studies have assumed the medium permeability to be isotropic for developing numerical models, despite isotropic geological media being uncommon in the real world. This study investigates the effect of medium permeability anisotropy on the morphological evolutions of two non-uniformities with higher permeability in a geochemical dissolution system. A series of numerical simulations are performed to evaluate the effect of medium permeability anisotropy on the morphological evolution of a chemical dissolution front. The simulation results indicate that the patterns of the dissolution reaction front are substantially affected by medium permeability anisotropy. An increase in the permeability anisotropy ratio, which is defined as the ratio of the permeability in the transverse direction to that in the longitudinal direction, enhances the dominance of the flow-focusing effect over the stabilizing or merging effect induced by diffusion/dispersion mechanism. Therefore, an increase in the permeability anisotropy ratio can increase the fingering length of the dissolution front or cause the dissolution front to have a more unstable pattern. By contrast, a reduction in the permeability

anisotropy ratio will weaken the flow-focusing effect, thereby reducing the fingering length of the dissolution front or changing the front morphology such that it has a more stable status. The effect of the permeability anisotropy ratio on the morphological evolution tends to decrease when the Zhao number (negative dimensionless upstream pressure gradient) of the system increases. The consideration of medium permeability anisotropy in the geochemical dissolution model renders the simulation of the morphological evolutions of dissolution reaction fronts more realistic.

- **Previous** article
- **Next** article

Keywords

Chemical dissolution front
Medium permeability anisotropy
Stable planar front
Unstable single-fingering front
Unstable double-fingering front
Flow-focusing effect

1. Introduction

When groundwater flows through a geological medium, mass transfer between aqueous and solid phases occurs because of various heterogeneous chemical reactions. Among such heterogeneous chemical reactions, the dissolution and precipitation reactions are the most important; these two reactions cause appreciable mass transfer between solid and aqueous phases, and also alter both the porosity and permeability of the geological medium.

If small non-uniformities with high permeability, which are common in real geological media, exist initially in a real geological medium, groundwater preferentially flows through these high-permeability zones. The increased groundwater flow causes a faster local dissolution, which in turn enhances the porosity and permeability of the zones. Consequently, flow in low-permeability zones is laterally captured to these high-permeability zones, resulting in a flow-focusing effect (Fig. 1). The flow-focusing effect tends to amplify non-uniformities and causes them to develop into unstable fingering reaction fronts. Molecular diffusion/mechanical dispersion resulting from a concentration gradient may inhibit the flow-focusing effect, preventing the unstable fingering reaction front from elongating indefinitely (Chadam et al., 1986, Ortoleva et al., 1987a, Ortoleva et al., 1987b, Zhao et al., 2008a, Zhao et al., 2008c, Zhao, 2014).

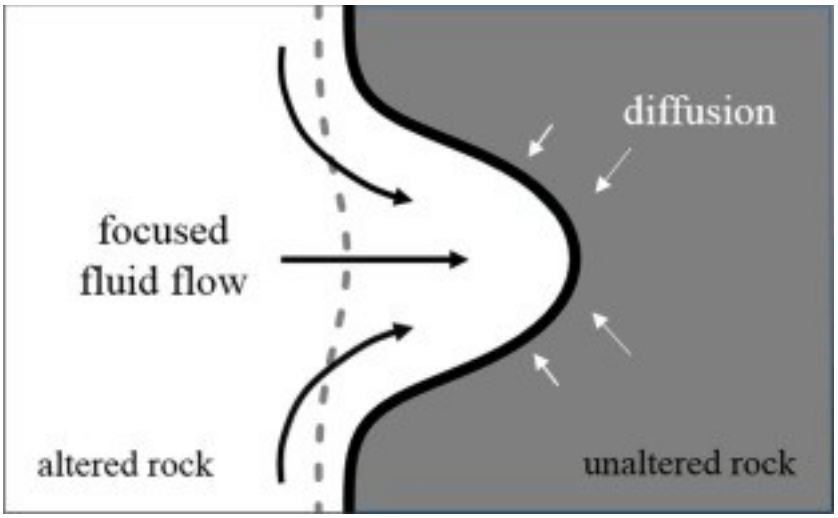

1. Download high-res image (44KB)
2. Download full-size image

Fig. 1. Competition of flow-focusing mechanism with diffusion. The gray dashed line represents the initial position of chemical dissolution front.

The morphological evolution of chemical reaction fronts induced by a dissolution reaction was initially investigated by Ortoleva and his coauthors in the late 1980s (Chadam et al., 1986, Ortoleva et al., 1987a, Ortoleva et al., 1987b). Chadam et al. (1986) performed a numerical simulation to demonstrate such a dissolution-induced fingering reaction front phenomenon by numerically solving a set of fully coupled nonlinear governing partial differential equations for groundwater flow, chemical species transport and porosity change induced by mineral dissolution. However, Zhao et al. (2008a) noticed that some governing equations derived by Chadam et al. (1986) were incorrect due to two conceptual mistakes: including (1) the confusion between the average linear velocity and Darcy velocity for a fluid-saturated medium and (2) the neglect of the dissolved mineral shape, and they re-derived the governing equations to correct those errors. After Zhao et al. (2008a) corrected these two conceptual mistakes, they have conducted extensive and pioneering research, both theoretically and numerically, to investigate how several factors such as reactive surfaces of particles (Zhao et al., 2008b), mechanical dispersion (Chen et al., 2009a, Zhao et al., 2010a), mineral dissolution ratios (Zhao et al., 2010b), medium/fluid compressibility (Zhao et al., 2012a, Zhao et al., 2012b), the permeability–porosity relationships (Lai et al., 2014) and temperature effect (Zhao et al., 2015a, Zhao et al., 2015b) affect the morphological evolution of reaction fronts within geological media in the field of the emerging computational geosciences (Zhao et al., 2009). As a result, the first monograph on this topic was published in the world (Zhao, 2014), indicating that a complete theoretical

framework has been established on the chemical dissolution-front instability in porous media. In addition, the relevant numerical simulations have also conducted by others (Chen et al., 1990, Chen et al., 2009b, Ortoleva, 1994, Renard et al., 1998, Chen and Liu, 2002, Chen and Liu, 2004, Zhao et al., 2013b).

Researchers in previous studies have often assumed the medium permeability to be the same in all direction (i.e., isotropic) for developing numerical models, despite the permeability commonly being anisotropic in real geological media. An anisotropic medium means that the permeability at a point varies in different directions. In general, medium permeability anisotropy is caused in real geological media because of (1) preferential lithological and crystal alignments; (2) irregularly shaped particles; (3) stress-induced effects; (4) aligned cracks; and (5) size, geometry, roughness, and circularity of soil pores. In a sedimentary medium, which comprises several layers with various thicknesses and permeabilities, the equivalent vertical and horizontal permeabilities can be easily computed mathematically if each layer is considered to be individually isotropic and homogeneous (Zhao et al., 2013a). The ratio of equivalent horizontal permeability to equivalent vertical permeability typically ranges from 2 to 10. Therefore, we can theoretically assume that the sedimentary medium is anisotropic. A numerical model that assumes the medium permeability isotropy may not be appropriate for correctly simulating the morphological evolutions of chemical dissolution fronts if medium permeability anisotropy is common in the real world.

More recently, Lai and Chen (2011) and Zhao et al. (2013a)found that medium permeability anisotropy can affect the morphological evolutions of a dissolution pattern. Zhao et al. (2013a) were the first to derive an analytical solution and establish a theoretical criterion for a critical condition, which is used to determine if the chemical dissolution front can become unstable. They also modified their numerical model used in previous studies by considering medium permeability anisotropy to investigate how medium permeability anisotropy affects the morphological development of a planar chemical dissolution front in a two-dimensional fluid-saturated porous medium. Their theoretical and numerical results indicated that a reduction in the medium permeability anisotropy ratio, which is defined as the ratio of the principal permeability in the transverse direction to that in the longitudinal direction (i.e. in the pore-fluid flow direction), can stabilize the chemical dissolution front, implying that it is more difficult for a planar reaction front to evolve into unstable fingering front patterns in a geochemical dissolution system.

Chen and Liu (2004) simulated the interaction of two non-uniformities in a chemical dissolution system and reported that the two non-uniformities developed into a stable

planar front, unstable single-fingering front, and unstable double-fingering front at a low Zhao number (which is defined as the minus value of the dimensionless upstream pressure gradientat the entrance of the chemical dissolution system), medium Zhao number, and high Zhao number, respectively. They used primary and secondary critical Zhao numbers to explain the dependence of morphological patterns on the upstream pressure gradient. Note that since the Zhao number is a dimensionaless number, which can be used to represent the three major controlling mechanisms (i.e. pore-fluid flow, mass transport and chemical reactions) simultaneously taking place in a chemical dissolution system (Zhao et al., 2013a), it has a clear physical meaning and therefore can be used to replace the upstream pressure gradient.

Thus, to obtain further insight into the morphological evolution of a dissolution reaction front, we extended the study of Chen and Liu (2004) to investigate how permeability anisotropy of an aquifer influences the temporal development of two non-uniformities in a geochemical dissolution system. The permeability anisotropy was included in the coupled governing equation system for describing the porosity change induced by a dissolution reaction, groundwater flow, and reactive solute transport, and a numerical model was constructed. Subsequently, a series of numerical simulations were performed to illustrate the effects of the permeability anisotropy on the morphological development of the chemical dissolution front. We further demonstrated the physical basis of the development of reactive dissolution fronts subjected to various permeability anisotropy values by quantitatively analyzing the advective, diffusive/dispersive, and the resultant chemical species flux. Crucial conclusions based on simulation results were drawn.

2. Mathematical model

This section presents a brief description of the numerical model that is used to evaluate the impact of the aquiferpermeability anisotropy on the morphological evolution of the two non-uniformities. The numerical model is developed on the basis of nonlinear partial differential equations for describing the dynamics of changes in medium porosity in relation to the mineral dissolution reaction, groundwater flowand transport of chemical species in a fluid-saturated porous medium. The underlying assumptions are summarized as follows (Zhao et al., 2008a, Zhao, 2014): (1) a single solid component and a single aqueous chemical species in an ideal geological medium are considered; (2) the porous medium comprises pores and soluble and insoluble grains; (3) the grain geometry is spherical; (4) mineral dissolution does not change the number of soluble grains; (5) groundwater flow and species diffusive/dispersive transport obey Darcy's law

and Fick's law, respectively; and (6) the dissolution reaction occurs according to the first-order kinetic rate equation.

If the velocity in the x direction is considerably greater than that in the y direction, the coupled partial differential equations (in 2D Cartesian coordinates) governing porosity changes resulting from the dissolution reaction, groundwater flow, and reactive transport of chemical species can be expressed as follows (Zhao et al., 2008a, Zhao, 2014):

(1)$\partial\phi\partial t=\Gamma nB1/3\alpha sphere(\phi f-\phi)2/3(ceq-c)$

(2)$\partial\phi\partial t=\partial\partial x\psi xx(\phi)\partial p\partial x+\partial\partial y\psi yy(\phi)\partial p\partial y$

(3)$\partial(\phi c)\partial t=\partial\partial x(aL\psi xx(\phi)\partial p\partial x+dm(\phi))\partial c\partial x+\psi xx(\phi)\partial p\partial xc+\partial\partial y(aT\psi xx(\phi)\partial p\partial x+dm(\phi))\partial c\partial y+\psi yy(\phi)\partial p\partial yc+\rho s\Gamma nB1/3\alpha sphere(\phi f-\phi)2/3(ceq-c)$

where t is time, x and y are spatial coordinates, ϕ is the porosity, p is the pore-water pressure, c is the species concentration in the groundwater, ϕf is the final porosity after complete dissolution of soluble grains, ceq is the equilibrium concentration of the dissolvable mineral, Γ is the rate constant of the chemical dissolution reaction, nB is the number density of the soluble grains, $\alpha sphere$ is the shape coefficient of the spherical grains, $\psi xx(\phi)=kxx(\phi)/\mu$, $\psi yy(\phi)=kyy(\phi)/\mu$, $kxx(\phi)$ is the porosity-dependent permeability in the inflow direction, $kyy(\phi)$ is the porosity-dependent permeability in the transverse direction, μ is the dynamic viscosity of water, ρs is the solid molar density of soluble mineral, aL is the longitudinal dispersivity, aT is the transverse dispersivity, $dm(\phi)$ is diffusion coefficient.

A modified form of the Fair–Hatch relation is adopted in the current study to characterize the dependence of the permeability on porosity (Chadam et al., 1986, Chen and Liu, 2002, Lai et al., 2014):

(4)$k(\phi)=\phi 3E2[(1-\phi)2/3+E1(\phi f-\phi)2/3]2$

where E1 and E2 are constants.

The common relation for the dependence of the molecular diffusion on porosity was presented by Bear (1972):

(5)$Dm(\phi)=Di\phi M32<M<52$

where Di is the diffusion coefficient in pure water.

In most natural geological system, the mineral dissolution ratio (Zhao et al., 2010b) is very small; therefore, a large time span is required for a porosity change in a geochemical reaction system. A scale parameter defined as the mineral dissolution ratio (Zhao et al., 2010b) can be mathematically expressed as follows:

$\varepsilon=ceq\rho s<<1$

When ε is incorporated to shift the time variable and then the dimensionless variables X=Γ·nB1/3ceqαsphereϕfdm(ϕf)·x, Y=Γ·nB1/3ceqαsphereϕfdm(ϕf)·y, T=ΓnB1/3ceqαsphereε·t, C=cceq, P=ψ(ϕf)ϕfdm(ϕf)·p, Ψ(ϕ)=ψ(ϕ)ψ(ϕf), Dm(ϕ)=ϕdm(ϕ)ϕfdm(ϕf), AL=Γ·nB1/3ceqαsphereϕfdm(ϕf)·aL, AT=Γ·nB1/3ceqαsphereϕfdm(ϕf)·aT

Eqs. (1), (2), (3) can then be expressed as follows:

(6)εϕ∂T=(ϕf-ϕ)2/3(1-C)

(7)εϕ∂T=∂X∂ΨXX(ϕ)∂PX+∂Y∂ΨYY(ϕ)∂PY

(8)ε∂(ϕc)∂T=∂X∂(ALΨXX(ϕ)∂PX+Dm(ϕ))∂CX+ΨXX(ϕ)∂PXC+∂Y∂(ALΨXX(ϕ)∂PX+Dm(ϕ))∂CY+ΨYY(ϕ)∂PYC+1ε(ϕf-ϕ)2/3(1-C)

We consider a two-dimensional benchmark problem to provide insights into how the medium permeability anisotropy affects the morphological evolution of two non-uniformities. Fig. 2 shows the geometry and simulation setup for the 2D benchmark problem. The length and height of the simulated rectangular domain are LX and LY, respectively. The top and bottom boundaries of the simulated domain are impermeable to fluid flow and reactive species. A dimensionless pressure gradient is applied to the left boundary to ensure that the horizontal groundwater flows into the simulated system from the left. Moreover, the inflow is under-saturated with respect to the reactive mineral phase, and the value of the inlet concentration is assumed to be constant.

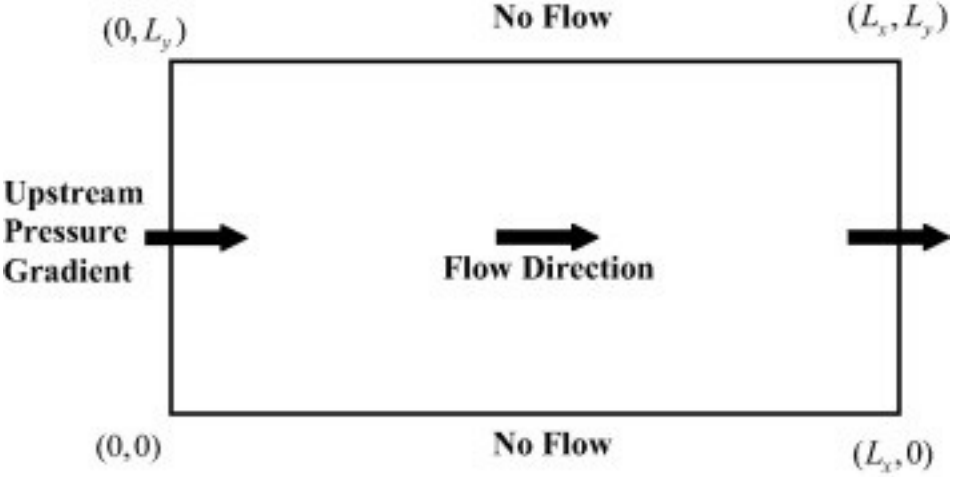

1. Download high-res image (64KB)
2. Download full-size image

Fig. 2. The geometry and the simulation setup for the two-dimensional dissolution benchmark problem. Groundwater from left enters the system.

The boundary conditions associated with Eqs. (6), (7), (8) can be mathematically expressed as follows:

(9)∂P(X=0,Y,T)∂X=-Pf

(10)P(X=LX,Y,T)=0

(11)∂P(X,Y=0,T)∂Y=0

(12)∂P(X,Y=LY,T)∂Y=0

(13)C(X=0,Y,T)=C0

(14)∂C(X=LX,Y,T)∂X=0

(15)∂C(X,Y=0,T)∂Y=0

(16)∂C(X,Y=LY,T)∂Y=0

where Pf is the negative dimensionless pressure gradient applied to the left boundary (which can be also denoted as the Zhao number, *Zh*).

A perturbed non-uniformity condition is required to trigger the development of the dissolution reaction front. In this study, the perturbed condition of two non-uniformities is applied. The two non-uniformities are generated by assuming the porosity of the porous medium and the concentration are initially homogeneous throughout the simulation domain, except in local zones of higher porosity and under-saturated concentration at (X=0, Y=LY/2+a) and (X=0, Y=LY/2-a), respectively. This means that the spacing between the two non-uniformities is 2a.

The initial condition for the porosity and dimensionless concentration are expressed as follows:

(17)ϕ(X,Y,T=0)=ϕ0+(ϕf-ϕ0)[e-ξ1+e-ξ2]

(18)C(X,Y,T=0)=(1-e-5X)(1-e-ξ2-e-ξ2]

where

ξ1(X,Y)={X4+[Y-(LY/2-a)]4}/(wLY)4ξ2(X,Y)={X4+[Y-(LY/2+a)]4}/(wLY)4

The coupled nonlinear partial differential equations (i.e., Eqs. (6), (7), (8)), together with the boundary conditions and initial conditions (i.e., Eqs. (9), (10), (11), (12), (13), (14), (15), (16), (17), (18)), are solved using an implicit finite difference method and the implicit sequential iteration approach (SIA). The SIA is used to solve each of the coupled nonlinear equations individually in a sequential manner. The SIA can be used to reduce the size of coefficient matrix considerably. Yeh and Tripathi (1989) indicated that the implicit SIA can be used to accelerate numerical convergence. Details of the numerical procedures used in this study can be found in Appendix A.

3. Results and discussion

The proposed model is used to investigate the effect of medium permeability anisotropy on the morphological evolution of the two initial non-uniformities in the geochemical dissolution system. The input parameters used to simulate the morphological growth of the two local non-uniformities are listed as follows:

initial porosity $\phi 0=0.1$, final porosity $\phi f=0.2$, inflow concentration $C0=0$, length $LX=18$, height $LY=8$, porosity dependent permeability constant $E1=1$, porosity dependent permeability constant $E2=1$, porosity dependent diffusion constant $M=2$, solid molar density of mineral $\varepsilon=0.05$, the Zhao number Zh = 0.75, 1.5, 2.5, 3, 6, and 10, and initial perturbation parameter, ω = 0.1. Chen et al. (2009a) investigated the effects of mechanical dispersion on the morphological evolution of dissolution reaction fronts. The longitudinal and transverse dispersivityare set to be zero in this study. Three medium anisotropicpermeability ratios, kyy/kxx = 1/9, 1, and 9 are used.

As demonstrated by Chen and Liu (2004), the two initial local non-uniformities may progress to form a stable planar front, unstable single-fingering front, or unstable double-fingering front, depending on the Zhao number and the spacing between the two non-uniformities. For a fixed spacing, a stable planar front is formed when the Zhao number is lower than the primary critical Zhao number. A single-fingering front emerges when the Zhao number is between the primary and secondary critical Zhao numbers. A double-fingering front is formed when the Zhao number is greater than the secondary critical Zhao number.

A series of numerical simulations with various permeability anisotropy ratios are conducted for diverse upstream pressure gradients by considering a fixed non-uniformity spacing of 3. Fig. 3 shows a comparison of the temporal evolution of dissolution fronts for a geological medium with different permeability anisotropy ratio (kyy/kxx) and for Zh = 0.75, 1.5, 2.5, 3, 6 and 10. Some vital aspects of the numerical simulations are described herein.

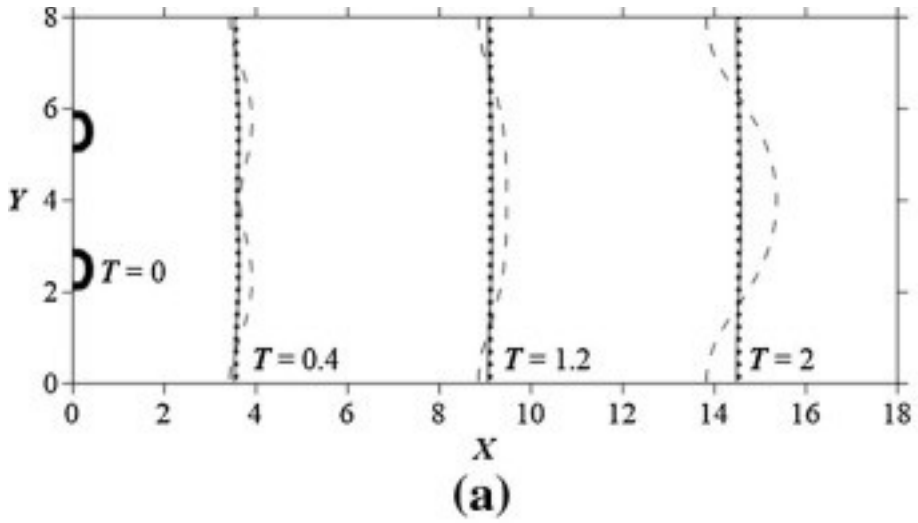

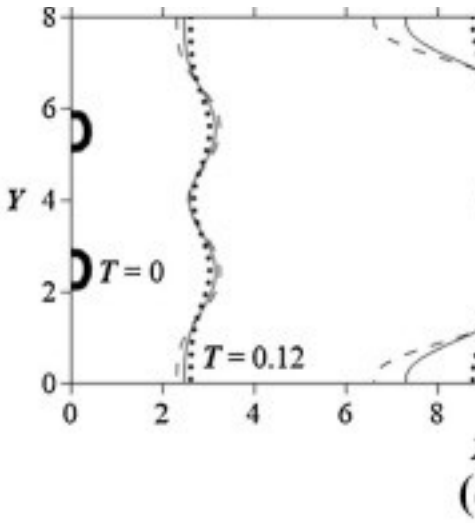

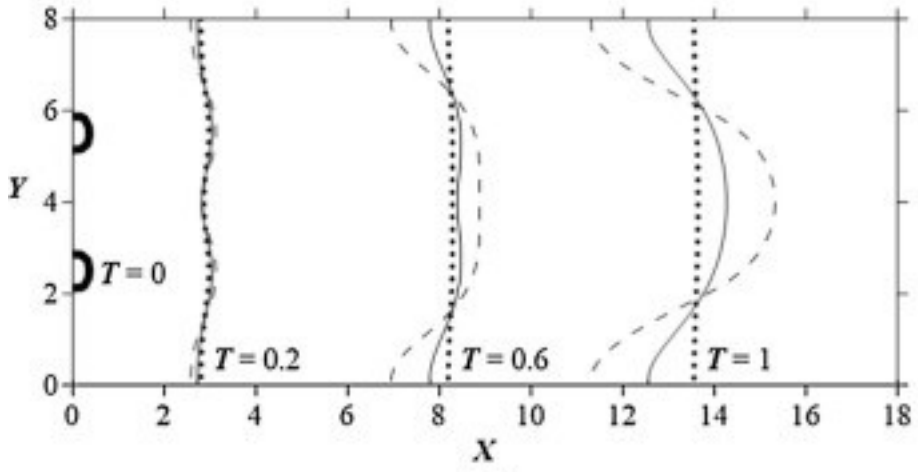

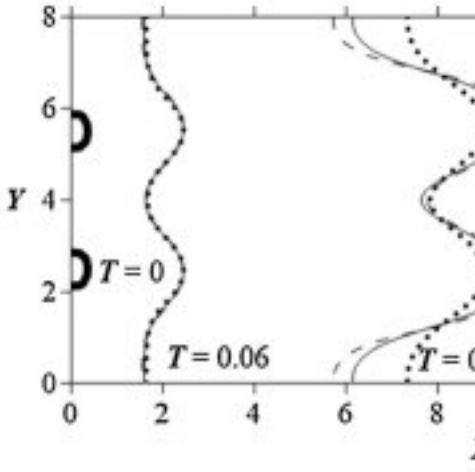

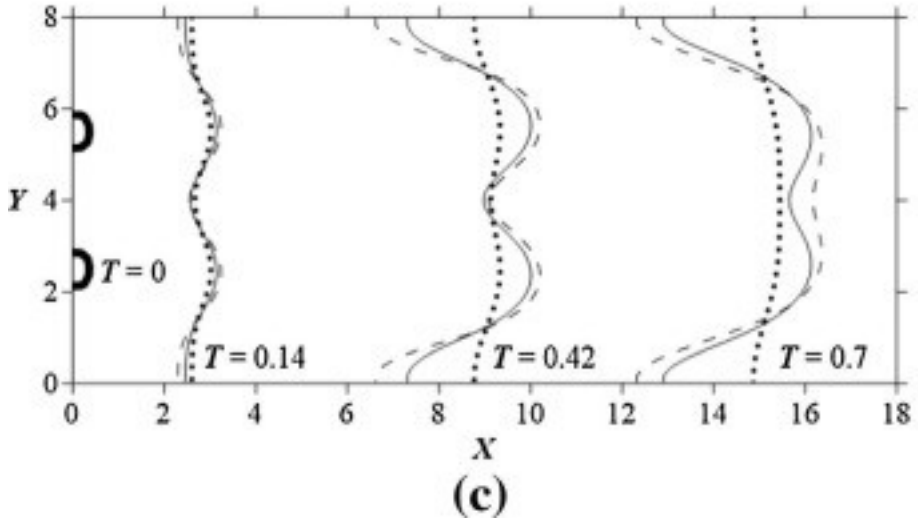

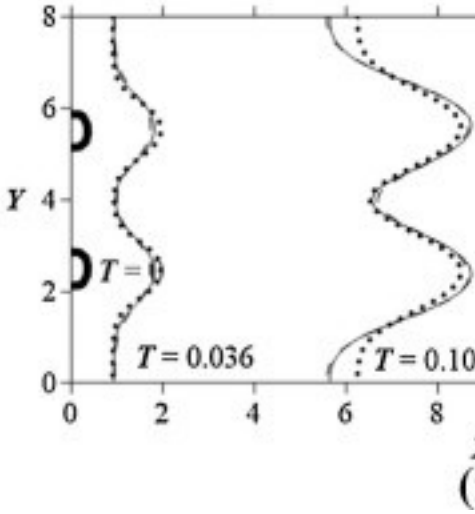

1. Download high-res image (248KB)

2. Download full-size image

Fig. 3. Temporal evolution of medium porosity contours (iso-line $(\phi 0+\phi f)/2=0.15$) for a porous medium with two initial non-uniformity (fixed spacing of 3) under Zh = (a) 0.75; (b) 1.5; (c) 2.5; (d) 3; (e) 6; (f) 10. Dotted line: $kyy/kxx=1/9$; Solid line: $kyy/kxx=1$; dashed line: $kyy/kxx=9$.

When Zh = 0.75, a stable planar front is formed for both kyy/kxx = 1 and 1/9, but an unstable single fingering front emerges for kyy/kxx = 9 (Fig. 3a). A comparison of kyy/kxx = 9 with kyy/kxx = 1 (isotropic) indicated that an increase in the kyy/kxx value can result in an increase in the flow-focusing effect, thereby altering the competition between the flow-focusing effect and finger elongation-inhibited effect of the diffusion/dispersion mechanism. The two non-uniformities easily transforms into an unstable single-fingering front. To quantitatively illustrate the aforementioned competition, Fig. 4, Fig. 5, Fig. 6 show a comparison of the spatial distributions of the advective, diffusive/dispersive, and resultant species flux, respectively, for Zh = 0.75 and kyy/kxx = 1/9, 1, and 9. The arrows and their adjacent values represent the directions and magnitude of the species flux. A larger advective flux was observed near the front finger for kyy/kxx = 9, compared with that observed for kyy/kxx = 1/9 and 1, but the diffusive flux was nearly identical for all three cases. The resultant species flux is thus governed by the advective flux, which is determined by the permeability anisotropy value.

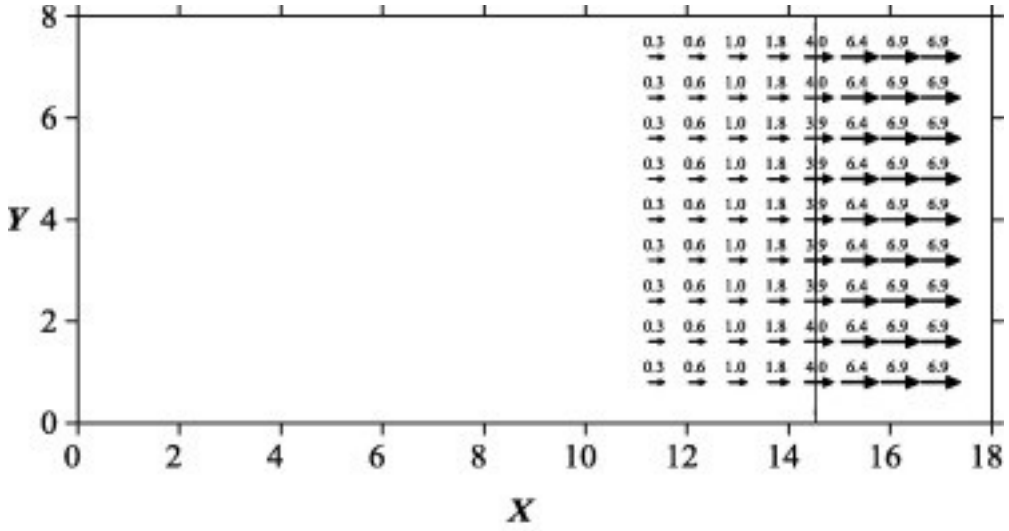
Y
X
0
2
4
6
8
10
12
14
16
18

(a)

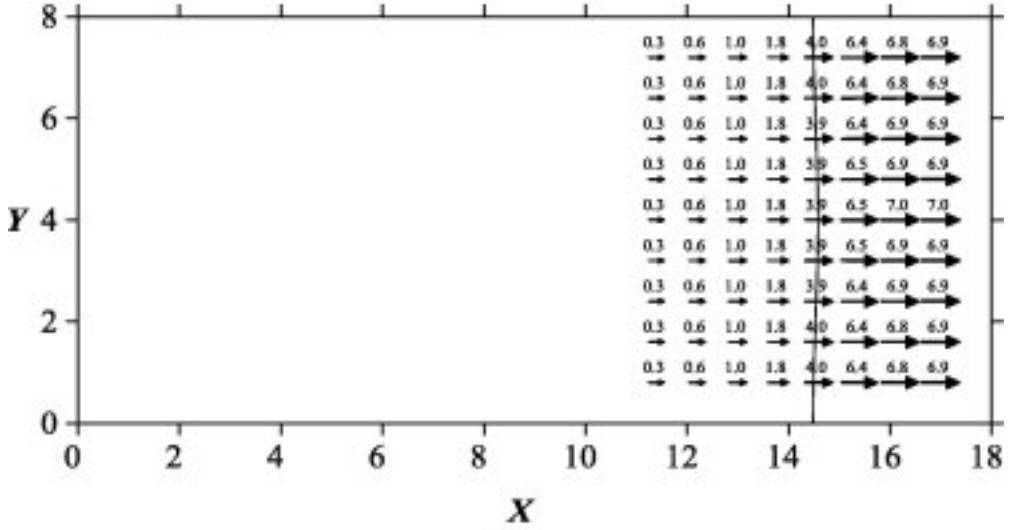
Y
X
0
2
4
6
8
10
12
14
16
18

(b)

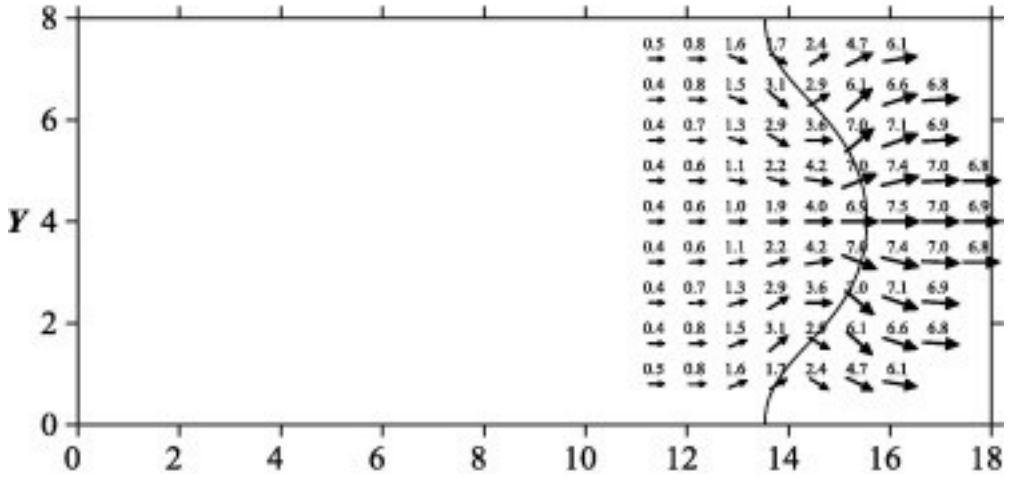
Y
0
2
4
6
8
10
12
14
16
18

1. Download high-res image (384KB)
2. Download full-size image

Fig. 4. Quantitative analysis of advective species fluxes of morphological evolution of two initial non-uniformity (fixed spacing of 3) under z_h = 0.75 at τ = 2 for (a) $k_{yy}/k_{xx=1/9}$; (b) $k_{yy}/k_{xx=1}$; (c) $k_{yy}/k_{xx=9}$.

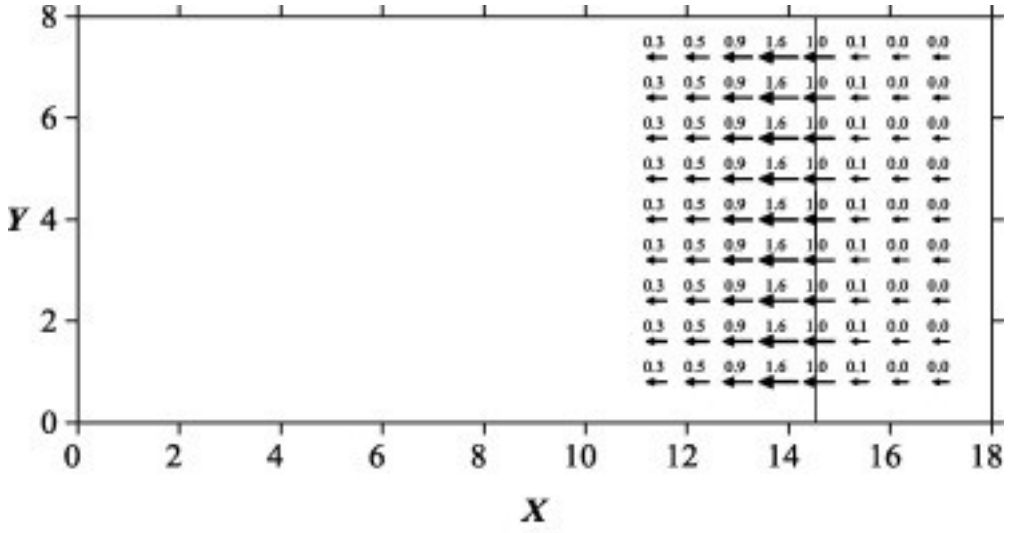
Y
X
0
2
4
6
8
10
12
14
16
18

(a)

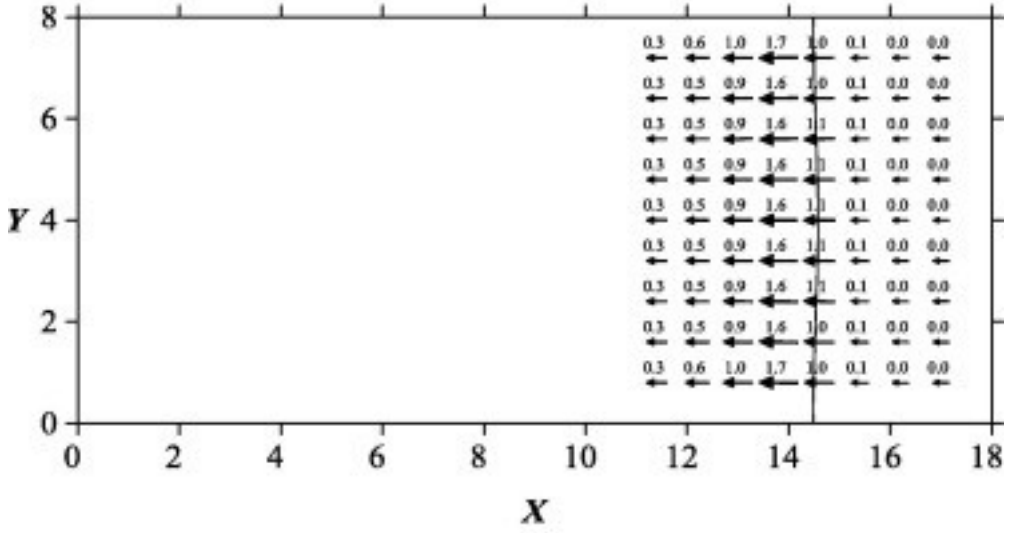
Y
X
0
2
4
6
8
10
12
14
16
18

(b)

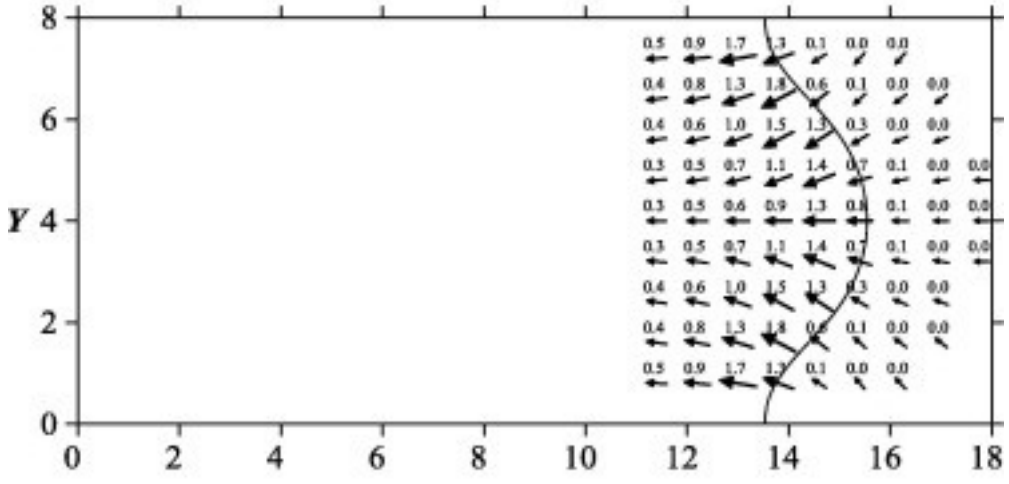
Y
0
2
4
6
8
10
12
14
16
18

1. Download high-res image (383KB)
2. Download full-size image

Fig. 5. Quantitative analysis of diffusive species fluxes of morphological evolution of two initial non-uniformity (fixed spacing of 3) under Z_h = 0.75 at τ = 2 for (a) $k_{yy}/k_{xx}=1/9$; (b) $k_{yy}/k_{xx}=1$; (c) $k_{yy}/k_{xx}=9$.

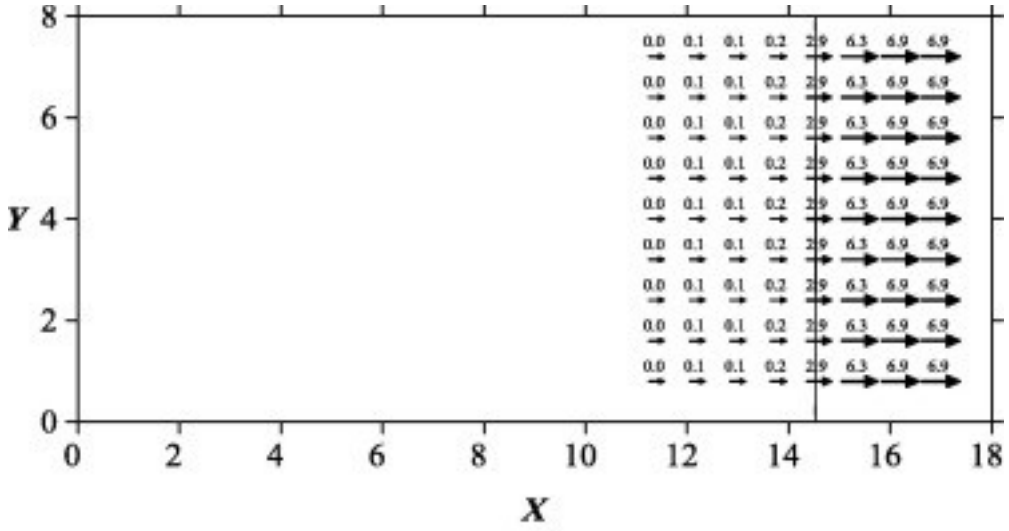
Y
X
0
2
4
6
8
10
12
14
16
18

(a)

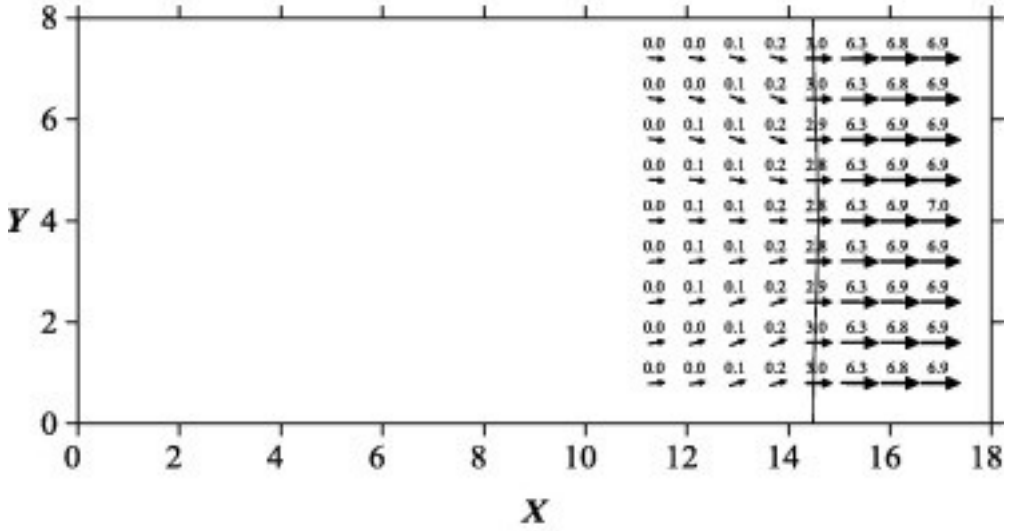
Y
X
0
2
4
6
8
10
12
14
16
18

(b)

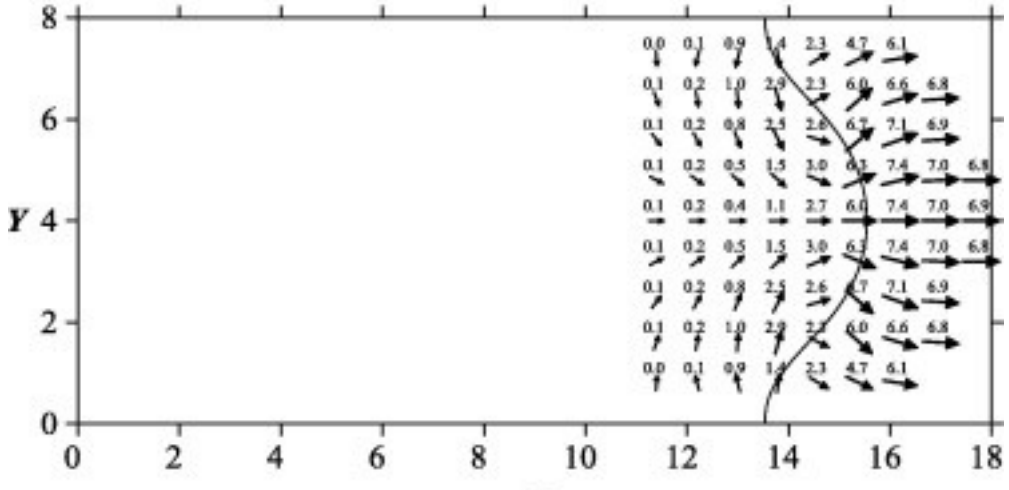
Y
0
2
4
6
8
10
12
14
16
18

1. Download high-res image (374KB)
2. Download full-size image

Fig. 6. Quantitative analysis of resultant species fluxes of morphological evolution of two initial non-uniformity (fixed spacing of 3) under Z_h = 0.75 at τ = 2 for (a) $k_{yy}/k_{xx=1/9}$; (b) $k_{yy}/k_{xx=1}$; (c) $k_{yy}/k_{xx=9}$.

Notably, when Z_h = 1.5, a stable planar front was remained for k_{yy}/k_{xx} = 1/9 and an unstable single-fingering front developed for k_{yy}/k_{xx} = 1 and 9 (Fig. 3b), with the protrusion for k_{yy}/k_{xx} = 9 being longer. Fig. 3b can be explained as follows: an increase in k_{yy}/k_{xx} strengthens the flow-focusing effect, and the competition of this effect against the finger elongation-inhibited effect, thus resulting an increase of the length of the unstable fingering front. By contrast, a reduction in k_{yy}/k_{xx} weakens the flow-focusing effect; therefore, the same magnitude of diffusion can inhibit the flow-focusing effect and stabilize the perturbation of the two non-uniformities to a planar front.

When the Z_h value is increased to 2.5, an unstable double-fingering front developed initially (T = 0.14); later, (T > 0.42) an unstable single-fingering front for k_{yy}/k_{xx} = 1/9 and an unstable double-fingering front for k_{yy}/k_{xx} = 1 and 9 were observed (Fig. 3c). A more prominent front is observed for k_{yy}/k_{xx} = 9 compared with the other cases. This means that when the permeability anisotropy ratio is increased to strength the flow-focusing effect, the development of the unstable double-fingering front is amplified; however, the permeability anisotropy ratio is reduced to weaken the flow-focusing effect, the dominance of the flow-focusing effect over the front-merging effect of diffusion is reduced, degenerating the unstable double-fingering front to an unstable single-fingering front.

When the Z_h value is continually increased to 3, similar to the case of Z_h = 2.5 more distinct patterns were produced. Specifically, an obscure single-fingering front for k_{yy}/k_{xx} = 1/9 and an evident double-fingering front for k_{yy}/k_{xx} = 1 and 9 were observed (Fig. 3d). No difference is perceived in the reaction fronts between the two value of k_{yy}/k_{xx} = 1 and 9, implying that the contribution of an increase in the permeability anisotropy ratio to the entire flow-focusing effect is not appreciable compared with that of high advective flux induced by a higher Z_h. The weakening of the flow-focusing effect induced by a reduction in the permeability anisotropy ratio can effectively suppress the dominance of flow-focusing effect over front merging effect by diffusion, leading to the degeneration of the unstable double-fingering front to an unstable single-fingering front.

When the Z_h value is continually increased to 6 and 10, all three cases show a clear double-fingering front (Fig. 3e and f). The dissolution fronts of k_{yy}/k_{xx} = 1 and 9

coincide. Although the finger length for kyy/kxx = 1/9 is shorter than that of the other cases, the differences among the three cases decreased as the Zh value increased. This is because the additional contribution of a change in the permeability anisotropy ratio to the entire flow-focusing effect is small compared with that of high advective flux induced by a higher Zh value. The higher the Zh value, the smaller is contribution of a change in the permeability anisotropy ratio to the flow-focusing effect. Fig. 7, Fig. 8, Fig. 9 illustrate a comparison of the spatial distributions of the advective, diffusive, and resultant species flux, respectively, for Zh = 10 for kyy/kxx = 1/9, 1, and 9. No considerable distinctions of flux patterns are observed among the three fluxes three cases. Specifically, unstable sharp dissolution fronts preferentially develop at high Zh, regardless of the permeability anisotropy value. Steefel and Lasaga (1990)applied the Damkohler number (ratio of the chemical reaction rate to the advective mass transport rate) to quantify the development of an unstable dissolution front. When the Damkohler number is lower then 1, the advective mass transport rate is higher than the reaction rate, resulting in development of an unstable dissolution fingering front. However, if the Damkohler number is greater than 1, the chemical reaction rate is higher than the fluid transport rate, resulting in a stable planar front. The Zhao number is thus the main physical parameter governing the morphological pattern in a geochemical dissolution system.

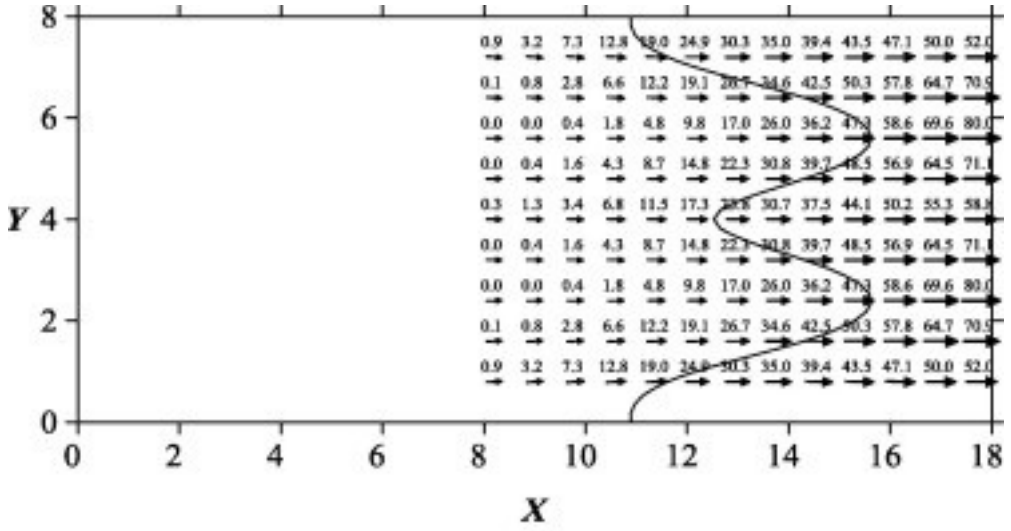
Y
X
0
2
4
6
8
10
12
14
16
18

(a)

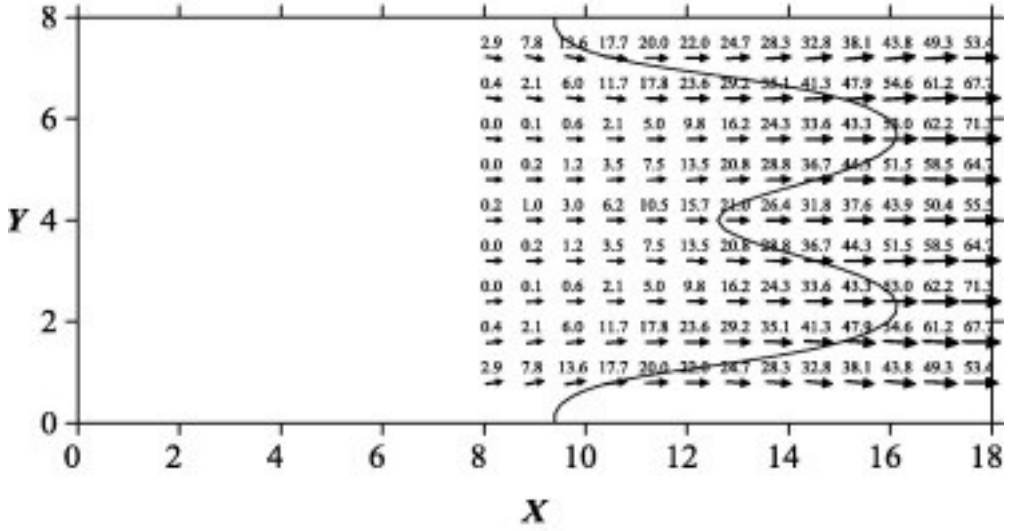
Y
X
0
2
4
6
8
10
12
14
16
18

(b)

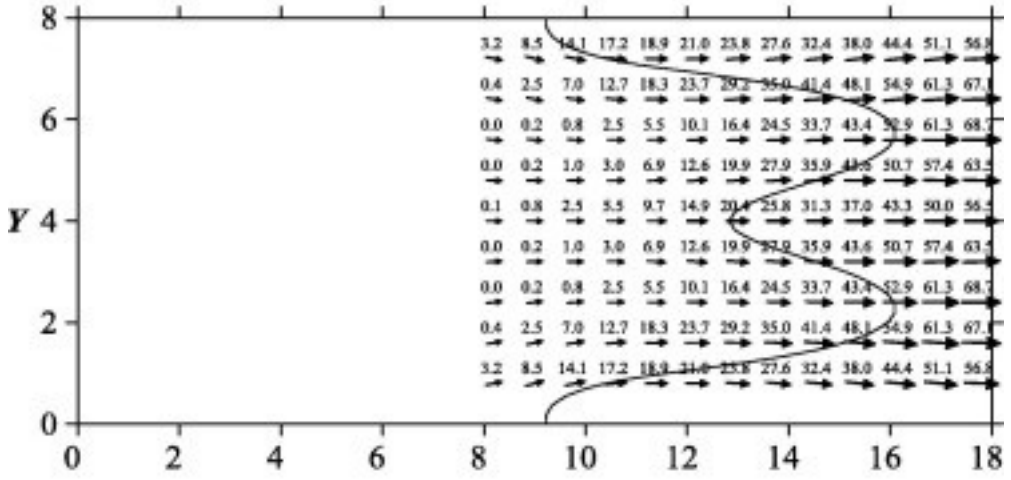
Y
0
2
4
6
8
10
12
14
16
18

1. Download high-res image (608KB)
2. Download full-size image

Fig. 7. Quantitative analysis of advective species fluxes of morphological evolution of two initial non-uniformity (fixed spacing of 3) under Z_h = 10 at τ = 0.18 for (a) $k_{yy}/k_{xx=1/9}$; (b) $k_{yy}/k_{xx=1}$; (c) $k_{yy}/k_{xx=9}$.

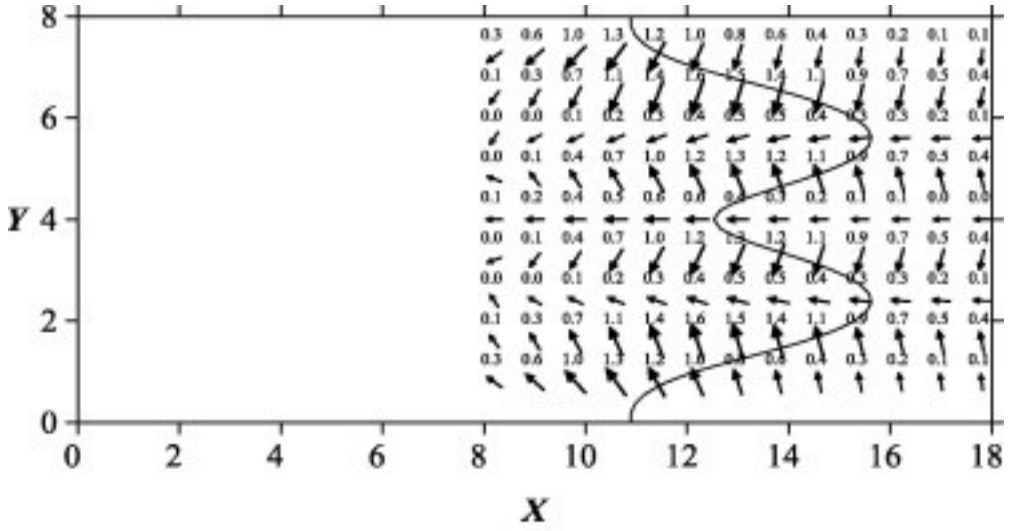
Y
X
0
2
4
6
8
10
12
14
16
18

(a)

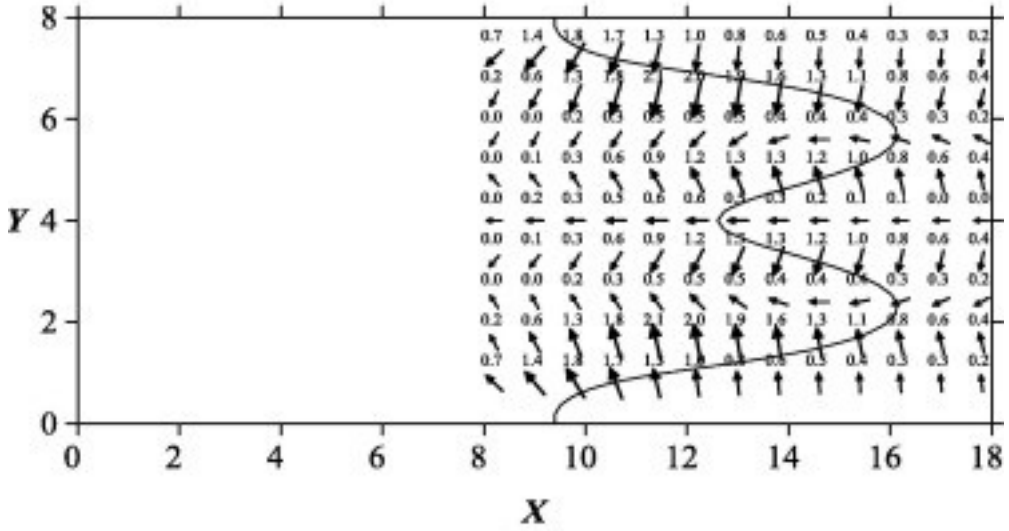
Y
X
0
2
4
6
8
10
12
14
16
18

(b)

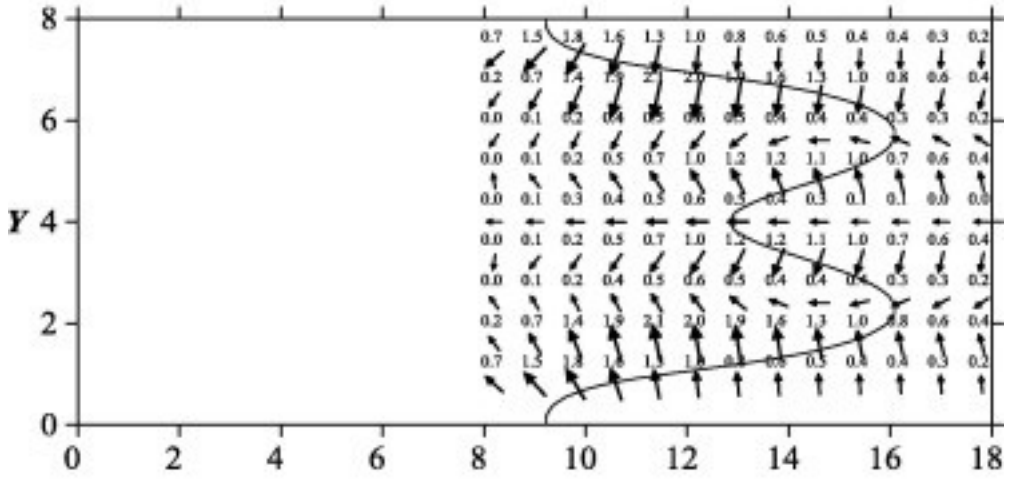
Y
0
2
4
6
8
10
12
14
16
18

1. Download high-res image (560KB)
2. Download full-size image

Fig. 8. Quantitative analysis of diffusive species fluxes of morphological evolution of two initial non-uniformity (fixed spacing of 3) under Z_h = 10 at τ = 0.18 for (a) $k_{yy}/k_{xx}=1/9$; (b) $k_{yy}/k_{xx}=1$; (c) $k_{yy}/k_{xx}=9$.

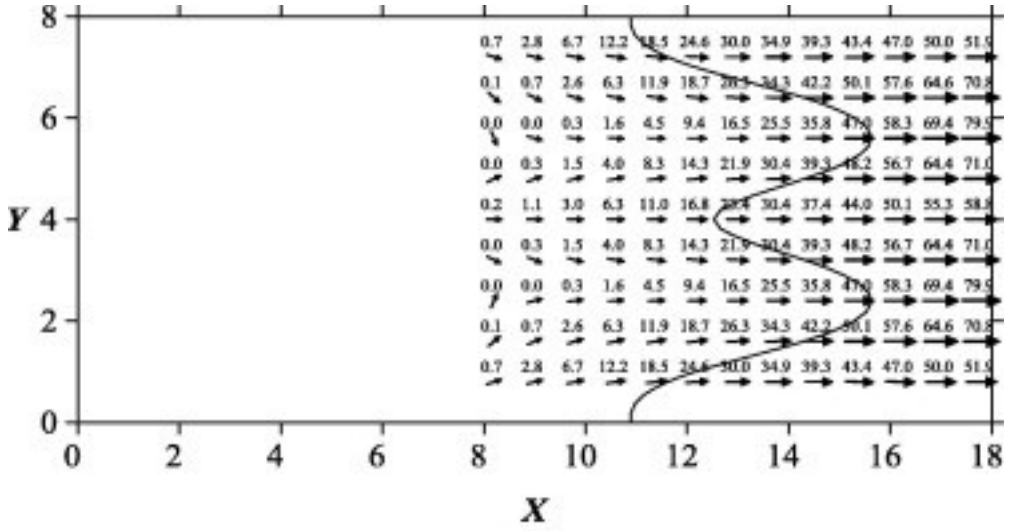
Y
X
0
2
4
6
8
10
12
14
16
18

(a)

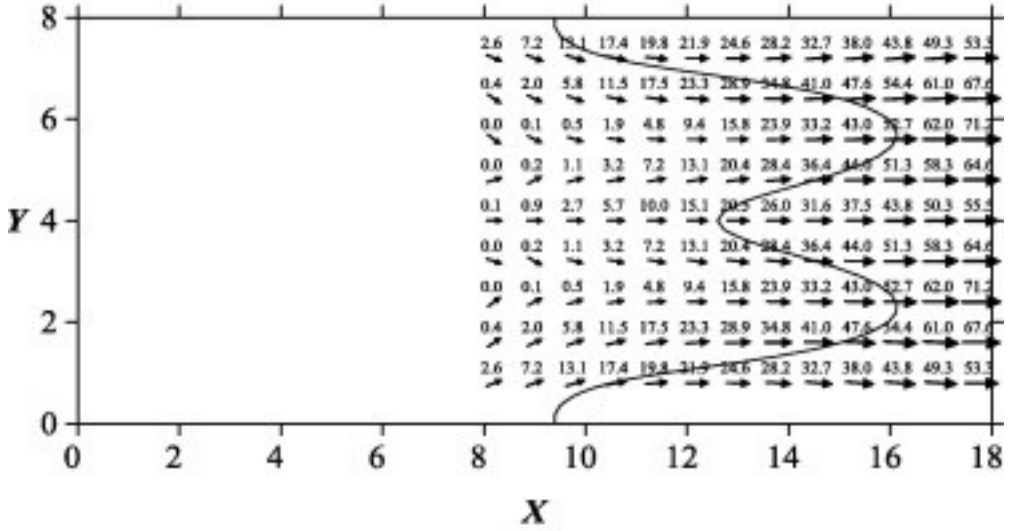
Y
X
0
2
4
6
8
10
12
14
16
18

(b)

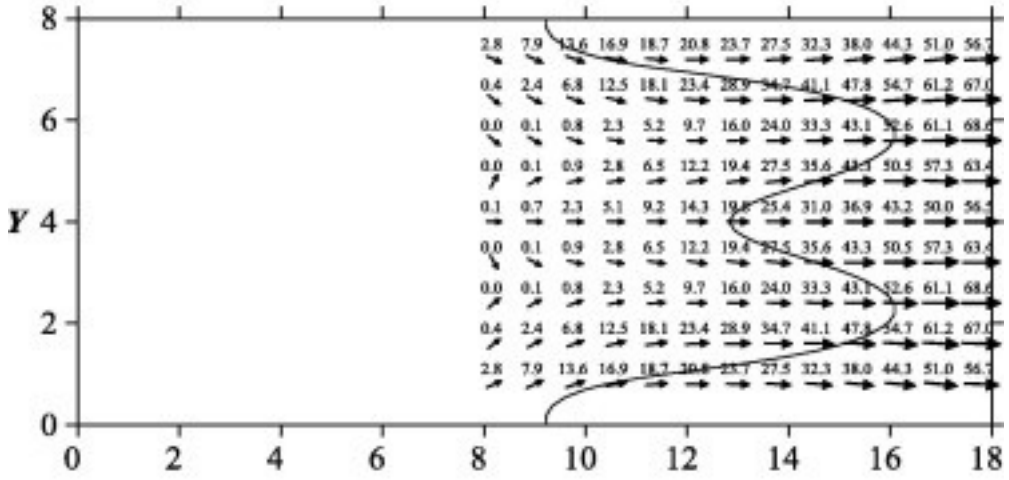
Y
0
2
4
6
8
10
12
14
16
18

1. Download high-res image (610KB)
2. Download full-size image

Fig. 9. Quantitative analysis of resultant species fluxes of morphological evolution of two initial non-uniformity (fixed spacing of 3) under Z_h = 10 at τ = 0.18 for (a) $k_{yy}/k_{xx=1/9}$; (b) $k_{yy}/k_{xx=1}$; (c) $k_{yy}/k_{xx=9}$.

Fig. 10 illustrates a two-dimensional behavior diagram that concludes the front morphologies in various medium anisotropy ratios and the Zhao numbers. A stable planar front is observed in both low medium anisotropy ratios and low Zhao numbers. An unstable single-fingering front occurs in a middle anisotropy ratio and low Zhao number, or in low medium anisotropy ratio and middle Zhao number. Moreover, the unstable double-fingering fronts can preferentially develop at high Zhao number regardless the permeability anisotropy values (i.e. the Zhao number greater than 3.5 in Fig. 10).

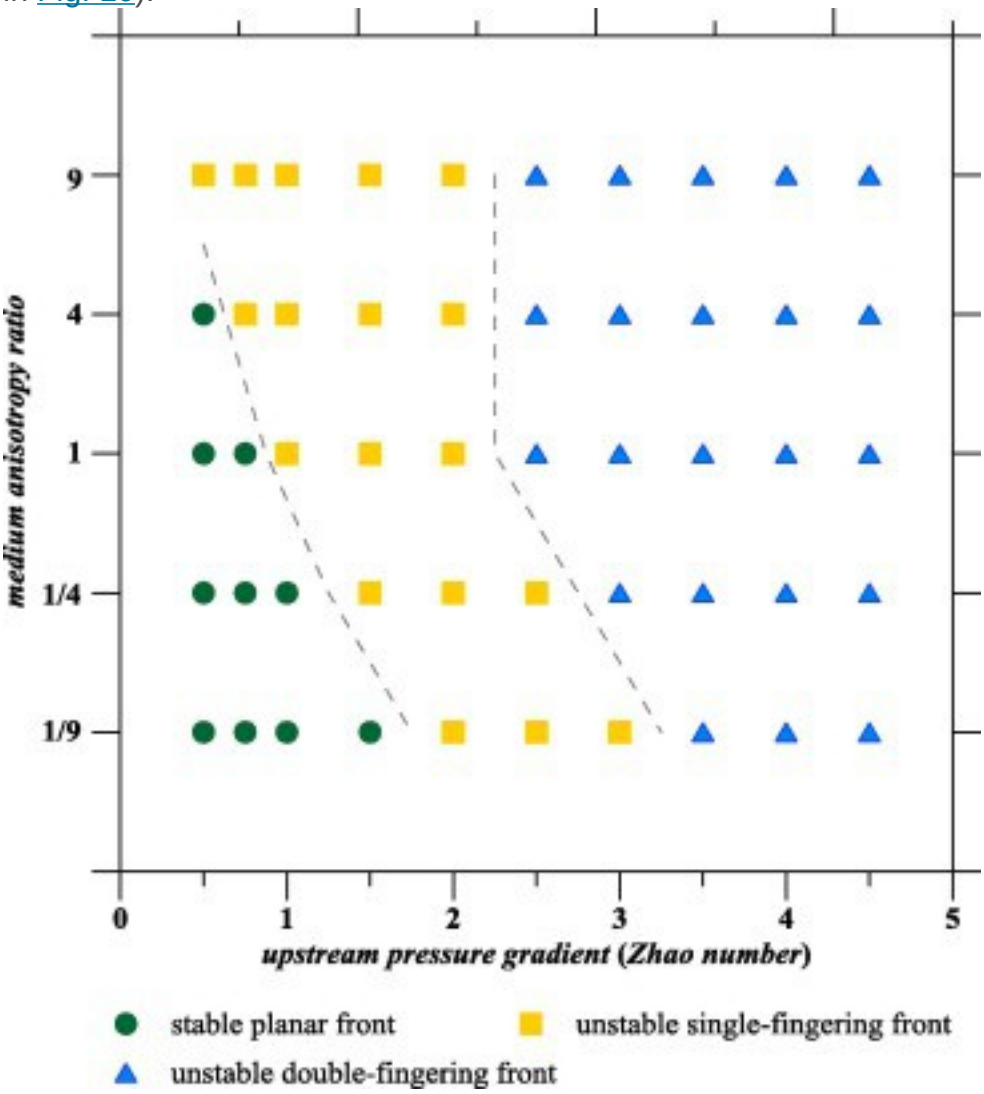

1. Download high-res image (163KB)
2. Download full-size image

Fig. 10. The behavior diagram summarizes that front morphologies are depended on medium permeability ratios and upstream gradient pressure (Zhao number). Circle represents the planar front; square represents the unstable single-fingering front; triangle represents the double-fingering front.

In summary, an increase in the medium permeability anisotropy ratio enhances the dominance of the flow-focusing effect over the fingering-inhibiting or fingering-merging effect, thereby increasing the tendency of the two non-uniformities to develop into an unstable single-fingering front or a double-fingering front. By contrast, a reduction in the medium permeability anisotropy ratio weakens the flow-focusing effect and reduces the competition between this effect and the fingering-inhibiting or fingering-merging effect, increasing the likelihood of the two non-uniformities stabilizing or merging to form a planar front or an unstable single-fingering front. Moreover, at a high Zhao number, variations in the medium permeability anisotropy ratio do not appreciably alter the morphological pattern of chemical dissolution fronts.

4. Conclusion

Medium permeability anisotropy is common in geological media and can play a crucial role in the development of a dissolution reaction front during geochemical dissolution reactive transport. However, most previous studies have only considered the isotropic medium. To in-depth understanding of the geochemical dissolution morphology, we investigate the morphological evolution of two initial non-uniformities by incorporating medium permeability anisotropy into a governing equation system. We perform a series of numerical simulations under various Zhao numbers and medium anisotropy ratios. The results show that temporal morphological pattern of the two non-uniformities is substantially influenced by the medium permeability anisotropy ratio. However, the effect of the medium permeability anisotropy on the dissolution front morphology decreases as the Zhao number increases. Quantitative analyses of advective, diffusive, and resultant species fluxes show that the self-focusing effect is enhanced when the medium permeability anisotropy ratio is greater than unity, thus destabilizing the two non-uniformities and resulting in the formation of an unstable single-fingering front or an unstable double fingering front. A two-dimensional behavior diagram that summarized the front morphologies in various medium anisotropy ratios and the Zhao numbers is conducted to delineate the stability of front development.

Acknowledgement

The author would like to thank the Ministry of Science and Technology of Taiwan for financially supporting this work under Contract No. NSC. 98-2313-B008-002-MY3.

Appendix A

The following steps describe an implicit SIA algorithm that advances a system of the discretized equations of Eqs. (6), (7), (8) from the *k*th time step to the (*k* + 1)th time step with a time increment ΔT.

A.1. Step 1

If $C_{i,j,kN}$ is initially provided, it can be substituted into the discretized equation of Eq. (6) to generate the (*N* + 1)th iteration porosity, $\phi_{i,j,kN+1}$. The discretized form of Eq. (6) may be rearranged as:

(A1) $\phi_{i,j,kN+1}=\phi_{i,j,k}+\phi f-\phi_{i,j,kN}+\phi_{i,j,k}22/31-C_{i,j,kN}+C_{i,j,k}2\Delta T\varepsilon.$

where subscript (i,j) denotes the grid center, and superscript *N* denotes the *N*th iteration for solving ϕ at time step k. The $C_{i,j,kN}$ can then be computed form the following:

$C_{i,j,kN}=C_{i,j,k},\text{if}N=1C_{i,j,kN}+C_{i,j,k}/2,\text{if}N>1$

A.2. Step 2

The computed porosity, $\phi_{i,j,kN+1}$, from Eq. (A1) can be directly substituted into the discretized form of Eq. (7) to generate (*N* + 1)th iteration pressure, $P_{i,j,kN+1}$. A semi-analytical derivative (Chen and Liu, 2002, Chen and Liu, 2004) is used to compute the spatial discretization of permeability:

(A2) $\partial\Psi XX(\phi)\partial Xi,j,kN+1=\partial\phi\partial X\partial\Psi XX(\phi)\partial\phi i,j,kN+1$

(A3) $\partial\Psi YY(\phi)\partial Yi,j,kN+1=\partial\phi\partial Y\partial\Psi YY(\phi)\partial\phi i,j,kN+1$

Then, the discretized form of Eq. (7) becomes:

(A4) $A1P_{i,j,kN+1}+A2P_{i+1,j,kN+1}+A3P_{i-1,j,kN+1}+A4P_{i,j+1,kN+1}+A5P_{i,j-1,kN+1}=A6,$

where

$A1=-2a2\Delta X2+-2a4\Delta Y2,A2=a2\Delta X2+a12\Delta X,A3=a2\Delta X2+-a12\Delta X,A4=a4\Delta Y2+a32\Delta Y,A5=a4\Delta Y2+-a32\Delta Y,A6=a5$

in which

$a1=\phi_{i+1,j,kN+1}-\phi_{i-1,j,kN+1}2\Delta X\partial\Psi XX(\phi)\partial\phi i,j,kN+1a2=\Psi XX(\phi)i,j,kN+1a3=\phi i,j+1,kn+1-\phi i,j-1,kn+12\Delta Y\partial\Psi YY(\phi)\partial\phi i,j,kN+1a4=\Psi YY(\phi)i,j,kN+1a5=\varepsilon\phi i,j,kN+1-\phi i,j,k\Delta T.$

A.3. Step 3

The (N + 1)th iteration concentration, $C_{i,j,kN+1}$, can be evaluated by substituting the $\phi_{i,j,kN+1}$ and $P_{i,j,kN+1}$ obtained from step 1 and 2 into the discretized form of Eq. (8). The spatial discretization of dispersion coefficients can be computed from (Chen et al., 2009a, Chen et al., 2009b)

(A5) $$\partial DL(\phi)\partial Xi,j,kN+1=AL\partial\phi\partial X\partial\Psi XX(\phi)\partial\phi\partial P\partial X+AL\Psi XX(\phi)\partial 2P\partial X2+\partial\phi\partial X\partial Dm(\phi)\partial\phi i,j,kN+1$$

and

(A6) $$\partial DT(\phi)\partial Yi,j,kN+1=AT\partial\phi\partial Y\partial\Psi XX(\phi)\partial\phi\partial P\partial X+AT\Psi XX(\phi)\partial 2P\partial X\partial Y+\partial\phi\partial Y\partial Dm(\phi)\partial\phi i,j,kN+1$$

The discretized form of Eq. (8) is expressed as:

(A7) $$B1Ci,j,kN+1+B2Ci+1,j,kN+1+B3Ci-1,j,kN+1+B4Ci,j+1,kN+1+B5Ci,j-1,kN+1=B6Ci,j,k+B7Ci+1,j,k+B8Ci-1,j,k+B9Ci,j+1,k+B10Ci,j-1,k+B11$$

$$B1=\varepsilon b1\Delta T+\varepsilon b2\Delta T+b4\Delta X2-b8b92-b10\Psi XX(\phi)|i,j,kN+12+b6\Delta Y2-b12b132-b14\Psi YY(\phi)|i,j,kN+12,B2=-b34\Delta X-b42\Delta X2-b7b94\Delta X,B3=b34\Delta X-b42\Delta X2+b7b94\Delta X,B4=-b54\Delta Y-b62\Delta Y2-b11b134\Delta Y,B5=b54\Delta Y-b62\Delta Y2+b11b134\Delta Y,B6=\varepsilon b1\Delta T-\varepsilon b2\Delta T-b4\Delta X2+b8b92+b10\Psi XX(\phi)|i,j,k2-b6\Delta Y2+b12b132+b14\Psi YY(\phi)|i,j,k2,B7=b34\Delta X+b42\Delta X2+b7b94\Delta X,B8=-b34\Delta X+b42\Delta X2-b7b94\Delta X,B9=b54\Delta Y+b62\Delta Y2+b11b134\Delta Y,B10=-b54\Delta Y+b62\Delta Y2-b11b134\Delta Y,B11=b1$$

in which

$$b1=\phi i,j,kN+1+\phi i,j,k2,b2=\phi i,j,kN+1-\phi i,j,k2,b3=\partial DL(\phi)\partial Xi,j,kN+1,b4=DL(\phi)i,j,kN+1+DL(\phi)i,j,k2,b5=\partial DT(\phi)\partial Yi,j,kN+1,b6=DT(\phi)i,j,kN+1+DT(\phi)i,j,k2,b7=\Psi XX(\phi)i,j,kN+1+\Psi XX(\phi)i,j,k2,b8=\partial\Psi XX(\phi)\partial Xi,j,kN+1,b9=Pi+1,j,kN+1+Pi+1,j,k2-Pi-1,j,kN+1+Pi-1,j,k22\Delta X,b10=Pi+1,j,kN+1+Pi+1,j,k2-2Pi,j,kN+1+Pi,j,k2+Pi-1,j,kN+1+Pi-1,j,k2\Delta X2,b11=\Psi YY(\phi)i,j,kN+1+\Psi YY(\phi)i,j,k2,b12=\partial\Psi YY(\phi)\partial Yi,j,kN+1b13=Pi,j+1,kN+1+Pi,j+1,k2-Pi,j-1,kN+1+Pi,j-1,k22\Delta Y,b14=Pi,j+1,kN+1+Pi,j+1,k2-2Pi,j,kN+1+Pi,j,k2+Pi,j-1,kN+1+Pi,j-1,k2\Delta Y2,b15=\phi i,j,kN+1-\phi i,j,k\Delta T.$$

A.4. Step 4

After implementing the procedures of steps 1–3, the solutions of $\phi_{i,j,kN+1}$, $P_{i,j,kN+1}$, and $C_{i,j,kN+1}$ are used as the new guess value for the next iteration. The steps 1–3 are iteratively repeated until the following convergence criterion is met:

(A8) $$\lambda i,j,kN+1-\lambda i,j,kN/\lambda i,j,kNmax\leqslant\xi\lambda,$$

where λ refers to ϕ, P, or C; $\xi\lambda$ is a specified residue constant; and the subscript “max” denotes the maximum value over all grid centers. At the end of the iteration, the values of $\phi_{i,j,k+1}$, $P_{i,j,k+1}$, and $C_{i,j,k+1}$ at time level k + 1 are assumed to be $\phi_{i,j,kN+1}$, $P_{i,j,kN+1}$, and $C_{i,j,kN+1}$, respectively.

References

Bear, 1972

J. Bear**Dynamics of Fluids in Porous Media**
Elsevier, Amsterdam (1972)
Chadam et al., 1986
J. Chadam, D. Hoff, E. Merino, P. Ortoleva, A. Sen**Reactive infiltration instabilities**
IMA J. Appl. Math., 36 (3) (1986), pp. 207-221
CrossRefView Record in Scopus
Chen et al., 1990
W. Chen, J. Chadam, P. Ortoleva**Morphological instabilities in physico-chemical systems**
Earth Sci. Rev., 29 (1–4) (1990), pp. 175-181
CrossRefView Record in Scopus
Chen and Liu, 2002
J.S. Chen, C.W. Liu**Numerical simulation of the evolution of aquifer porosity and species concentrations during reactive transport**
Comput. Geosci., 28 (4) (2002), pp. 485-499
ArticleDownload PDFView Record in Scopus
Chen and Liu, 2004
J.S. Chen, C.W. Liu**Interaction of reactive fronts during transport in a homogeneous porous medium with initial small non-uniformity**
J. Contam. Hydrol., 72 (1–4) (2004), pp. 47-66
ArticleDownload PDFView Record in Scopus
Chen et al., 2009a
J.S. Chen, C.W. Liu, G.X. Lai, C.F. Ni**Effects of mechanical dispersion on the morphological evolution of a chemical dissolution front a fluid-saturated porous medium**
J. Hydrol., 373 (2009), pp. 96-102
ArticleDownload PDFView Record in Scopus
Chen et al., 2009b
J.S. Chen, Y.Y. Chang, C.W. Liu**Evaluation of front morphological development of reactive solute transport using behavior diagrams**
Terrest., Atmos. Ocean. Sci., 20 (6) (2009), pp. 853-862
CrossRefView Record in Scopus
Lai and Chen, 2011
Lai, K.H., Chen, J.S., 2011. Effect of Permeability Anisotropy on Morphological Evolution of a Chemical Dissolution Front in a Fluid-saturated Porous Medium. Poster Session Presented at European Geosciences Union General Assembly 2011, Vienna, Austria.
Lai et al., 2014
K.H. Lai, J.S. Chen, C.W. Liu, S.Y. Yang**Effect of porosity–permeability functions on simulated morphological evolution of a chemical dissolution front**
Hydrol. Process., 28 (2014), pp. 16-24
CrossRefView Record in Scopus

Ortoleva, 1994

P. Ortoleva**Geochemical Self-organization**

Oxford University Press, New York (1994)

Ortoleva et al., 1987a

P. Ortoleva, J. Chadam, E. Merino, A. Sen**Self-organization in water-rock interaction systems: II. The reactive-infiltration instability**

Am. J. Sci., 287 (1987), pp. 1008-1040

CrossRefView Record in Scopus

Ortoleva et al., 1987b

P. Ortoleva, E. Merino, C. Moor, J. Chadam**Geochemical self-organization: I. Feedback mechanisms and modelling approach**

Am. J. Sci., 287 (1987), pp. 979-1007

CrossRef

Renard et al., 1998

F. Renard, J.P. Gratier, P. Ortoleva, E. Brosse, B. Bazin**Self-organization during reactive fluid flow in a porous medium**

Geophys. Res. Lett., 25 (3) (1998), pp. 385-388

CrossRefView Record in Scopus

Steefel and Lasaga,

1990

Steefel, C.L., Lasaga, A.C., 1990. The evolution of dissolution patterns: permeability change due to coupled flow and reaction. In: Melchior, D., Bassett, R.L. (Eds.), Chemical Modeling of Aqueous System II. ACS Symposium Series No. 416. American Chemical Society: Washington, pp. 212–255.

Yeh and Tripathi, 1989

G.T. Yeh, V.S. Tripathi**A critical evaluation of recent developments of hydrogeochemical transport models of reactive multichemical components**
Water Resour. Res., 25 (1) (1989), pp. 93-108
CrossRefView Record in Scopus

Zhao, 2014

C. Zhao**Physical and Chemical Dissolution Front Instability in Porous Media: Theoretical Analyses and Computational Simulations**
Springer, Berlin (2014)

Zhao et al., 2009

C. Zhao, B.E. Hobbs, A. Ord**Fundamentals of Computational Geoscience: Numerical Methods and Algorithms**
Springer, Berlin (2009)

Zhao et al., 2010

C. Zhao, B.E. Hobbs, A. Ord**Theoretical analyses of the effects of solute dispersion on chemical-dissolution front instability in fluid-saturated porous media**
Transp. Porous Media, 84 (3) (2010), pp. 629-653
CrossRefView Record in Scopus

Zhao et al., 2012

C. Zhao, B.E. Hobbs, A. Ord**Effects of medium and pore-fluid compressibility on chemical-dissolution front instability in fluid-saturated porous media**
Int. J. Numer. Anal. Meth. Geomech., 36 (2012), pp. 1077-1100
CrossRefView Record in Scopus

Zhao et al., 2013

C. Zhao, B.E. Hobbs, A. Ord**Effects of medium permeability anisotropy on chemical-dissolution front instability in fluid-saturated porous media**
Transp. Porous Media, 99 (1) (2013), pp. 119-143
CrossRefView Record in Scopus

Zhao et al., 2013
C. Zhao, B.E. Hobbs, A. Ord**Theoretical analyses of acidization–dissolution front instability in fluid-saturated carbonate rocks**
Int. J. Numer. Anal. Meth. Geomech., 37 (2013), pp. 2084-2105
CrossRefView Record in Scopus

Zhao et al., 2015
C. Zhao, B.E. Hobbs, A. Ord**Theoretical analyses of chemical dissolution-front instability in fluid-saturated porous media under non-isothermal conditions**
Int. J. Numer. Anal. Meth. Geomech., 39 (2015), pp. 799-820
CrossRefView Record in Scopus

Zhao et al., 2015
C. Zhao, B.E. Hobbs, A. Ord**Computational simulation of chemical dissolution-front instability in fluid-saturated porous media under non-isothermal conditions**
Int. J. Numer. Meth. Eng., 102 (2015), pp. 135-156
CrossRefView Record in Scopus

Zhao et al., 2008
C. Zhao, B.E. Hobbs, A. Ord, P. Hornby, S. Peng**Effect of reactive surface areas associated with different particles shapes on chemical-dissolution front instability in fluid-saturated porous medium**
Transp. Porous Media, 73 (1) (2008), pp. 75-94
CrossRefView Record in Scopus

Zhao et al., 2008
C. Zhao, B.E. Hobbs, A. Ord, P. Hornby, S. Peng**Morphological evolution of three-dimensional chemical dissolution front in fluid-saturated porous media: a numerical simulation approach**
Geofluids, 8 (2) (2008), pp. 113-127
CrossRefView Record in Scopus

Zhao et al., 2008
C. Zhao, B.E. Hobbs, A. Ord, P. Hornby, S. Peng**Theoretical and numerical analyses of chemical-dissolution front instability in fluid-saturated porous rocks**
Int. J. Numer. Anal. Meth. Geomech., 32 (9) (2008), pp. 1107-1130
CrossRefView Record in Scopus

Zhao et al., 2010
C. Zhao, B.E. Hobbs, A. Ord, B.E. Hornby, S. Peng**Effects of mineral dissolution ratios on chemical-dissolution front instability in fluid-saturated porous media**
Transp. Porous Media, 82 (2) (2010), pp. 317-335
CrossRefView Record in Scopus

Zhao et al., 2012

C. Zhao, L.B. Reid, K. Regenauer-Lieb, T. Poulet**A porosity-gradient replacement approach for computational simulation of chemical-dissolution front propagation in fluid-saturated porous media including pore-fluid compressibility**

Comput. Geosci., 16 (2012), pp. 735-755

CrossRefView Record in Scopus

Recommended articles

- Development and calibration of a reactive transport model for carbonate reservoir porosity and permeability changes based on CO_2 core-flood experiments

  International Journal of Greenhouse Gas Control, Volume 57, 2017, pp. 73-88
  Download PDFView details
- Modelling karst aquifer evolution in fractured, porous rocks

  Journal of Hydrology, Volume 543, Part B, 2016, pp. 796-807
  Download PDFView details
- Chronostratigraphic confirmation of MIS 5 age of a baymouth bar at Is Arenas (Cagliari, Italy)

  Quaternary International, Volume 232, Issues 1–2, 2011, pp. 169-178
  Download PDFView details

12Next

Citing articles (7)

Article Metrics

Captures

- Readers:6

Social Media

- Tweets:1

Citations

- Citation Indexes:7

View details